Ameliorating Methylglyoxal-Induced Progenitor Cell Dysfunction for Tissue Repair in Diabetes

Hainan Li,[1] Megan O'Meara,[1] Xiang Zhang,[1] Kezhong Zhang,[2,3] Berhane Seyoum,[4] Zhengping Yi,[1,5] Randal J. Kaufman,[6] Terrence J. Monks,[1,5] and Jie-Mei Wang[1,2,7]

Diabetes 2019;68:1287–1302 | https://doi.org/10.2337/db18-0933

Patient-derived progenitor cell (PC) dysfunction is severely impaired in diabetes, but the molecular triggers that contribute to mechanisms of PC dysfunction are not fully understood. Methylglyoxal (MGO) is one of the highly reactive dicarbonyl species formed during hyperglycemia. We hypothesized that the MGO scavenger glyoxalase 1 (GLO1) reverses bone marrow-derived PC (BMPC) dysfunction through augmenting the activity of an important endoplasmic reticulum stress sensor, inositol-requiring enzyme 1α (IRE1α), resulting in improved diabetic wound healing. BMPCs were isolated from adult male *db*/*db* type 2 diabetic mice and their healthy corresponding control *db*/+ mice. MGO at the concentration of 10 μmol/L induced immediate and severe BMPC dysfunction, including impaired network formation, migration, and proliferation and increased apoptosis, which were rescued by adenovirus-mediated GLO1 overexpression. IRE1α expression and activation in BMPCs were significantly attenuated by MGO exposure but rescued by GLO1 overexpression. MGO can diminish IRE1α RNase activity by directly binding to IRE1α in vitro. In a diabetic mouse cutaneous wound model in vivo, cell therapies using diabetic cells with GLO1 overexpression remarkably accelerated wound closure by enhancing angiogenesis compared with diabetic control cell therapy. Augmenting tissue GLO1 expression by adenovirus-mediated gene transfer or with the small-molecule inducer trans-resveratrol and hesperetin formulation also improved wound closure and angiogenesis in diabetic mice. In conclusion, our data suggest that GLO1 rescues BMPC dysfunction and facilitates wound healing in diabetic animals, at least partly through preventing MGO-induced impairment of IRE1α expression and activity. Our results provide important knowledge for the development of novel therapeutic approaches targeting MGO to improve PC-mediated angiogenesis and tissue repair in diabetes.

One of the most devastating situations seen in patients with long-term diabetes is unhealed wounds in their lower extremities, which usually result in foot ulcers or even amputations (1). Currently, there is no satisfactory treatment for diabetic wounds. Bone marrow-derived progenitor cells (BMPCs) are the reservoir for vascular repair and angiogenesis, an ideal solution for therapeutic revascularization (2). However, the number and function of progenitor cells (PCs) from patients with type 1 and type 2 diabetes are reduced (3), representing a major challenge for developing autologous cell therapies for wound healing (4). Therefore, it is critical to determine the molecular triggers that compromise PC function and disrupt neovascularization in diabetes to develop therapeutic protocols for diabetic wounds.

Methylglyoxal (MGO) is a highly reactive dicarbonyl aldehyde predominantly formed during glucose and fructose metabolism (5). MGO binds with proteins, lipids, and DNA, forming advanced glycation end products (AGEs) and leading to cell dysfunction and organ damage (6). Free MGO is difficult to detect. However, on the basis of the detection of one type of MGO adduct, MGO-derived hydroimidazolone-1, plasma levels of MGO in healthy subjects are in the nanomolar range. In contrast, MG hydroimidazolone-1 can reach micromolar levels in patients with

[1]Department of Pharmaceutical Sciences, Eugene Applebaum College of Pharmacy and Health Sciences, Wayne State University, Detroit, MI
[2]Center for Molecular Medicine and Genetics, Wayne State University, Detroit, MI
[3]Department of Immunology and Microbiology, Wayne State University, Detroit, MI
[4]Division of Endocrinology, School of Medicine, Wayne State University, Detroit, MI
[5]Integrated Biosciences, Wayne State University, Detroit, MI
[6]Degenerative Diseases Program, Sanford Burnham Prebys Medical Discovery Institute, La Jolla, CA
[7]Cardiovascular Research Institute, Wayne State University, Detroit, MI

Corresponding author: Jie-Mei Wang, jiemei.wang@wayne.edu

Received 31 August 2018 and accepted 9 March 2019

This article contains Supplementary Data online at http://diabetes.diabetesjournals.org/lookup/suppl/doi:10.2337/db18-0933/-/DC1.

diabetes (7,8). Two recent studies have revealed that elevated levels of MGO in patients with type 1 and type 2 diabetes are closely associated with a high incidence of cardiovascular events (9,10). The proposed mechanisms of MGO-induced organ damage include interrupting insulin secretion and signaling (11), inducing inflammation and oxidative stress (12,13), and modifying the extracellular matrix (particularly collagens) (14), among others. Despite recognition of the detrimental roles of MGO in the pathogenesis of diabetes-associated complications, technical obstacles have hindered mechanistic studies with MGO. For example, most current in vitro studies use very high concentrations of MGO, frequently in the millimolar range, which severely limits their relevance to physiological conditions (15,16). An alternative approach to study MGO is to observe the rate-limiting enzyme that detoxifies MGO—glyoxalase 1 (GLO1) (17). Under physiological conditions, >99% of MGO is detoxified by GLO1 (6,18). Reduced GLO1 activity in the blood has been documented in patients with type 1 and type 2 diabetes with painful neuropathy (19). Overexpression of GLO1 in diabetic adipose-derived stem cells shows improved proangiogenic capacity in vitro and in vivo (20). However, the exact mechanisms by which physiopathological levels of MGO induce cell dysfunctions remain unclear.

Diabetes-related lipotoxicity and glucotoxicity impose a heavy burden on the endoplasmic reticulum (ER), triggering ER stress (21). The ER engages unfolded protein response (UPR) signaling to restore ER homeostasis (21). However, if the stress burden exceeds ER folding capacity, the UPR can initiate apoptotic cascades that lead to cell death. ER stress has been implicated in the onset and progression of diabetes, contributing to pancreatic β-cell loss and insulin resistance (22,23). Inositol-requiring enzyme 1α (IRE1α) is one of the major transmembrane ER sensor proteins. In the canonical UPR pathway, IRE1α acts as an RNase to generate an activated transcription factor of X-box binding protein 1 (XBP1), which subsequently induces expression of downstream UPR genes involved in protein folding and degradation (24). Additionally, IRE1α can initiate a process termed IRE1α-dependent decay in which selected mRNAs or microRNAs (miRs) are cleaved, leading to accelerated RNA degradation (25,26). The role of IRE1α in regulating vascular cellular activities is not yet fully understood. Our recent study demonstrated that the activity of IRE1α is significantly attenuated in diabetic BMPCs, contributing to impaired angiogenesis in vitro (4). Diabetic BMPCs with IRE1α gene overexpression have exhibited dramatically enhanced efficacy in healing cutaneous wounds (4). However, why the functionality of IRE1α in endothelial PCs is damaged in diabetes is completely unknown.

Herein, we compared BMPC function upon MGO exposure to that following exposure to high glucose or AGEs to identify molecular triggers of PC dysfunction. We also examined whether IRE1α RNase activity is directly impaired by MGO modification. GLO1 overexpression was used to scavenge MGO in vitro and in vivo. In addition, diabetic wounds were treated with small-molecule GLO1 inducers trans-resveratrol (tRES) and hesperetin (HESP) to assess whether pharmacological intervention targeting GLO1 could effectively improve wound healing. Elucidating the mechanisms underlying MGO-induced BMPC dysfunction should assist in revealing the underappreciated role of reactive carbonyl species–induced cellular damage in diabetes. Such knowledge should contribute to the development of novel therapeutic strategies to prevent vascular complications through scavenging of these highly reactive species.

RESEARCH DESIGN AND METHODS

Animals

Male type 2 diabetic mice (BKS.Cg-m$^{+/+}$Lepr^{db}/J, *db/db*, age 10–12 weeks, plasma glucose 429.20 ± 19.30 mg/dL) and their age- and sex-matched nondiabetic healthy littermates (BKS.Cg-m$^{-/-}$Lepdb/− lean, *db/+*, plasma glucose 142.10 ± 4.96 mg/dL) were purchased from the Jackson Laboratory (#000642). IRE1α$^{flox/flox}$ mice were generated as we previously described (27). The endothelial cell–specific *Ire1α* knockout mice, IRE1α$^{flox/flox}$ TEK-Cre^{+} (referred to as IRE1α^{ECKO}), were generated by crossing IRE1α$^{flox/flox}$ with transgenic mice expressing Cre recombinase under Tie-2 (*Tek*) promoter/enhancer (TEK-Cre) (#008863; The Jackson laboratory). Their IRE1α$^{flox/flox}$ TEK-Cre^{null} (referred to as IRE1α$^{flox/flox}$) were used as control. The deletion of IRE1α in Tie-2–expressing cells, such as endothelial cells, was confirmed by IRE1α staining in aortas (Supplementary Fig. 1). All animal experiments were performed according to Wayne State University institutional animal care and use committee guidelines.

Mouse BMPC In Vitro Culture and Treatments

In vitro expansion and characterization of BMPCs was carried out as we previously described (4,28). Mouse bone marrow mononuclear cells were isolated by gradient centrifugation and maintained in endothelial growth media (EGM-2) (cc-4176; Lonza). The adhering cells were cultured for 7 days before used for experiments. High glucose (25 mmol/L, using 5 mmol/L as control) and AGE (121800; Millipore Sigma) (200 μg/mL, using BSA [BP1600; Thermo Fisher Scientific] as control) treatment was based on previous reports (16,29). MGO (M0252; Sigma-Aldrich) at 10 μmol/L (using H_2O as control) was used to reflect estimated MGO adduct levels in plasma of patients with diabetes (30). MGO was delivered to BMPCs in serum-free EGM-2 for 2 h then followed by EGM-2 containing 0.3% BSA for 22 h (a total of 24 h). IRE1α^{ECKO} mice were generated as we previously described (27). Transfections of adenovirus carrying human *Glo1* gene (Ad-GLO1) (ADV209980; Vector Biolabs), *Cre* recombinase (Ad-Cre), human IRE1a gene (Ad-IRE1α), or *egfp* gene (Ad-green fluorescent protein [GFP]) (all three provided by K.Z.) were performed at a multiplicity of infection of 50 for 48 h as described previously (27).

Human PC In Vitro Culture

All clinical procedures were approved by the institutional review board of Wayne State University. Written consent was obtained. None of the participants had any significant health-related conditions other than diabetes. Peripheral blood mononuclear cells of the enrolled subjects were isolated by density gradient centrifugation and cultured the same way as mouse BMPCs. The adhering cells were collected for Western blot assay after 7-day culture. The baseline characteristics of control subjects and patients are shown in Supplementary Table 2.

Western Blot Analyses

Western blot analysis was performed as previously described (4). Total protein was extracted from BMPCs. Equal amounts of denatured protein (30 μg) were separated and transferred to polyvinylidene fluoride membrane. Immunoblotting was performed by using antibodies directed against each target molecule: IRE1α (rabbit anti-mouse IRE1α, 1:1,000, #3249; Cell Signaling Technology), phosphorylated IRE1α (Ser724) (rabbit anti-mouse IRE1α, 1:1,000, NB100-2323; NOVUS Biologicals), GLO1 (mouse anti-mouse, 1:500, sc-133144; Santa Cruz Biotechnology), GAPDH (mouse anti-mouse, 1:5,000, sc-32233; Santa Cruz Biotechnology), and β-actin (mouse anti-mouse, 1:10,000, #12262; Cell Signaling Technology). Secondary antibodies horseradish peroxidase goat anti-mouse IgG (1:10,000) (P/N 926-80010; Li-Cor) and horseradish peroxidase goat anti-rabbit IgG (1:6,000) (P/N 926-80011; Li-Cor) were incubated at room temperature for 1 h. Membrane-bound antibodies were detected by an enhanced chemiluminescence detection reagent (Western-Sure ECL Substrate, 926-95000; Li-Cor). The blot was read with a C-DiGit scanner (Li-Cor). Molecular band intensity was determined with Image Studio Lite version 5.2 (Li-Cor).

BMPC Functional Assays (Network Formation, Migration, Proliferation, and Apoptosis Assays)

In the network formation assay, BMPCs in EGM-2 were plated in a 48-well cell culture plate (5×10^4 cells/well) precoated with 160 μL of growth factor–reduced Matrigel matrix (356231; Corning) as previously described (31). Cell migration was evaluated by a scratch assay. Cell proliferation was evaluated using CellTiter 96 AQueous One Solution Cell Proliferation Assay Kit (G358C; Promega). Cell apoptosis was evaluated with Annexin V-FITC Apoptosis Detection Kit with Propidium Iodide (PI) Staining Solution (556547; BD Pharmingen) as described previously (31).

In Vitro IRE1α-Mediated RNA Cleavage Assay

Purified active human IRE1α protein (1 μg/μL) (aa468-end, E31-11G-10; SignalChem) was modified by MGO (100 μmol/L) in vitro at 37°C for 2 h. IRE1α incubated with H_2O served as control. We have identified that precursors miR-466 and miR-200 are RNA substrates of IRE1α (4). In this experiment, ~1 μg in vitro–transcribed RNA substrate (pre-miR-466:pre-miR-200 = 1:1) was incubated with 1 μg bioactive recombinant human IRE1 protein in a reaction buffer (K01-09-01; SignalChem) for 30 min at 37°C. The cleavage reactions were initiated by adding ATP (2.5 mmol/L) (A50-09-200; SignalChem). Reaction without ATP initiation served as loading control. The cleavage products were resolved on a 1.2% agarose gel and visualized by ethidium bromide staining. Weak bands indicated that RNA substrate was spliced.

Luciferase Promoter Activity Assays

Synthetic oligonucleotides of human IRE1α or GLO1 mRNA promoter region were cloned into a LightSwitch Promoter Reporter GoClone system (GLO1: S718376; IRE1: S720185; SwitchGear). After treatments, BMPCs were transfected with 20 ng of promotor vectors per 2×10^4 cells using Fugene transfection reagent (F200; SwitchGear) according to the manufacturer's protocol. After 24 h, luciferase activity was measured using LightSwitch Luciferase Assay Kit (LS010; SwitchGear) in a GloMax Explorer luminescence microplate reader (Promega). The firefly luciferase activity indicates the transcriptional activity of the cloned target.

BMPC Cell Therapy and Gene Therapy for Wound Healing In Vivo

A full-thickness excisional wound was created on dorsal skin using a 6-mm punch biopsy without damaging the underlying muscle, as we previously described (31). For BMPC therapies, 1×10^6 BMPCs with different gene manipulations were topically placed onto the wound bed immediately after punch. For GLO1 gene transfer, 10^8 plaque-forming units (pfu) of Ad-GFP or Ad-GLO1 in PBS were injected onto the wound edge in the panniculus carnosus layer immediately after punch, as previously described (4). For small-molecule GLO1 inducer therapy of tRES (1602105; Sigma) and HESP (W431300; Sigma) coformulation, freshly prepared 5 μmol/L tRES and 5 μmol/L HESP in PBS containing 0.002% DMSO (D4540; Sigma) or vehicle control (0.002% DMSO) was topically applied every other day (32). Immediately after, wounds were covered with a transparent oxygen-permeable wound dressing (Tegaderm film, 1624M; 3M Medical) and changed every other day. Wound closure was monitored and calculated as percent closed (y%) = [(area on day_0 − open area on day_x) / area on day_0] × 100, as previously described (31). On day 6 after wounding, wounds and the adjacent skin were collected for CD31 (rat anti-mouse CD31, 550274; BD Pharmingen) immunochemistry staining.

Statistics

All values are expressed as mean ± SD. The statistical significance of differences between the two groups was determined with Mann-Whitney *U* nonparametric test. When more than two treatments were compared, one-way ANOVA followed by Mann-Whitney post hoc testing

was used. For the in vivo wound closure data, two-way repeated-measures ANOVA followed by Bonferroni post hoc testing was used to compare both differences between treatments and time courses, as previously described (31). All the statistical analyses were performed using GraphPad Prism 7 software. In all tests, $P < 0.05$ was considered statistically significant.

RESULTS

Micromolar MGO Causes Immediate and Severe Damage to BMPC Function Compared With High Glucose and AGEs

Mouse BMPCs were cultured from bone marrow mononuclear cells. After 7 days of culture, these cells demonstrated endothelial cell–like morphology and behavior, such as the uptake of LDL and binding with lectin (Fig. 1*A*). They were positive for vascular endothelial (VE)-cadherin staining (Fig. 1*A*) and presented high levels of stem cell markers, such as sca-1 and CD34, and low levels of endothelial cell markers, such as flk1 (murine VE growth factor receptor 2) (Fig. 1*B*). These data support their endothelial precursor phenotype, which is consistent with our previous reports (4,31). To determine which aspect of hyperglycemia accounts for the functional loss of BMPCs, we examined the effect of high glucose, AGEs, and MGO on BMPC function. The relationships among these three are demonstrated in Fig. 1*C*. Although MGO significantly increased apoptosis (Fig. 1*D* and *E*) and decreased network formation (Fig. 1*F* and *G*) and migration (Fig. 1*H* and *I*) after 24 h of exposure, high glucose or AGEs did not show such a detrimental effect on cell function until 72 h (Fig. 1*D–I*). However, even after 72 h of exposure, the extent of high glucose– or AGE-induced reduction in network formation and migration was minor. These data suggest that micromolar MGO imposes immediate and severe inhibition of BMPC function.

BMPCs Possess a Limited Glyoxalase Defense System, the Augmentation of Which Improves Cell Function In Vitro

Although GLO1 is the key enzyme that detoxifies MGO in all mammalian cells, GLO1 expression levels vary in different organs and tissues. For example, energy-consuming cells, such as skeletal muscle cells (SMCs), possessed robust GLO1 protein expression (Fig. 2*A*). However, primary cultured mouse aortic endothelial cells (33) and BMPCs expressed <33% of GLO1 protein compared with SMCs (all from *db/+* mice) (Fig. 2*A*), suggesting limited capacity of endothelial lineage cells to detoxify MGO. Interestingly, BMPCs expressed more GLO1 protein compared with mature endothelial cells, which may help BMPCs to maintain their functionality as a reservoir for endothelial repair and regeneration under glycation stress. Ad-GLO1 was used to overexpress GLO1 protein expression in *db/+* BMPCs (Fig. 2*B*). Functional tests, including network formation (Fig. 2*C* and *D*) and proliferation (Fig. 2*E*) indicated that GLO1 overexpression significantly improved BMPC function. Conversely, small interfering (si)RNA against GLO1 (si-GLO1), which reduced GLO1 protein expression by ~40% (Fig. 2*F*), led to significantly decreased BMPC network formation in vitro (Fig. 2*G* and *H*). GLO1 protein expression in diabetic BMPCs was lower than that in healthy controls (Fig. 3*A*). With GLO1 overexpression (Fig. 3*B*) (~2.5-fold vs. *db/db* plus Ad-GFP measured by Western blot), *db/db* BMPCs displayed improved network formation (Fig. 3*C* and *D*), proliferation (Fig. 3*E*), and migration (Fig. 3*F* and *G*) and decreased the high apoptosis in diabetic BMPCs (Fig. 3*H* and *I*). Together, the data strongly suggest that GLO1 overexpression restores the proangiogenic activity of diabetic BMPCs.

Exposure of MGO Suppresses IRE1α Protein Expression

IRE1α is an essential protein in maintaining BMPC functional integrity in diabetes (4). IRE1α protein expression and IRE1α activation (phosphorylated IRE1α) were reduced in diabetic BMPCs (Fig. 4*A*). We generated IRE1α$^{-/-}$ BMPCs by infecting IRE1α$^{flox/flox}$ BMPCs with Ad-Cre (Fig. 4*B*). Functional tests indicated that IRE1α deletion resulted in increased apoptosis (Fig. 4*C*) and impaired network formation (Fig. 4*D*) but not proliferation compared with IRE1α$^{+/+}$ BMPCs (Fig. 4*E*). Next, we exposed *db/+* BMPCs to MGO for 24 h. Our results showed that MGO significantly reduced the IRE1α protein (Fig. 4*F*) and its active, phosphorylated form (Fig. 4*G*) without affecting *Ire1α* mRNA (Fig. 4*H*). Other ER stress sensors and mediators, including PERK, ATF6, and Bip, were not affected by MGO exposure (Fig. 4*I*). To test whether MGO diminished IRE1α activity through direct binding, the RNase activity of native IRE1α or MGO-modified IRE1α was measured using an in vitro IRE1α-mediated RNA cleavage assay. We previously established that precursor miRs pre-miR-200 and pre-miR-466 can be directly digested by IRE1α and are consequently upregulated as a result of IRE1α deficiency in diabetic BMPCs (4); therefore, pre-miR-200 and pre-miR-466 were chosen as RNA substrates for IRE1α. The RNA substrate was incubated with IRE1α (native or MGO modified). RNA without IRE1α (Fig. 4*J*, left lane) served as an intact RNA control. RNAs digested by intact IRE1α showed a weak band upon RNA electrophoresis, whereas RNAs digested by MGO-modified IRE1α were comparable to untreated RNA (Fig. 4*J*), suggesting that MGO damaged IRE1α RNase activity through direct modification. Furthermore, we overexpressed IRE1α by Ad-IRE1α transfection before MGO exposure (Fig. 4*K*). MGO-induced impairment in network formation could be partly reversed by IRE1α overexpression (Fig. 4*K* and *L*), suggesting a protective role for IRE1α on BMPC function under glycation stress.

GLO1 Overexpression Rescues IRE1α Protein Expression and Activation

To determine whether scavenging MGO can rescue IRE1α protein expression and activation, Ad-GLO1 was used to

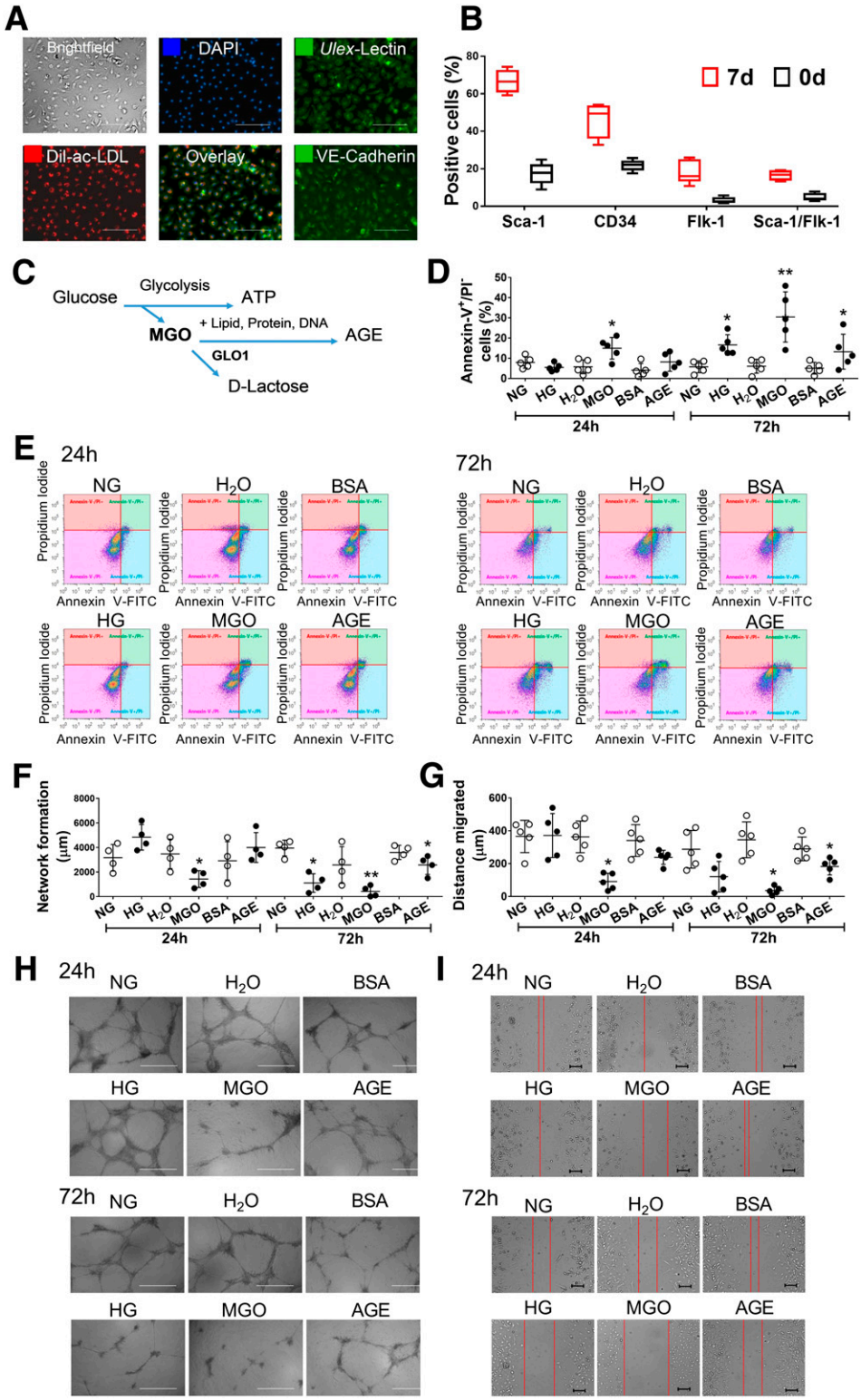

Figure 1—BMPC function was directly damaged by 24-h exposure of MGO rather than high glucose (HG) or AGEs. BMPCs from type 2 diabetic *db*/*db* mice and the healthy control *db*/+ mice were cultured in vitro for 7 days. *A*: Fluorescent staining of Ulex-lectin binding and DiI-ac-LDL uptake and VE-cadherin in 7-day cultured BMPCs (n = 4 per group). Scale bar = 500 μm. *B*: Flow cytometry analysis of Sca-1, CD34, Flk-1, CD45, and Sca-1/Flk-1 cell surface markers of BMPCs after 7 days of culture (n = 5 per group). BMPCs were then treated with either MGO (10 μmol/L, using H_2O as control), AGEs (200 μmol/L, using BSA as control), or HG (25 mmol/L D-glucose, using 5 mmol/L D-glucose plus 20 mmol/L D-mannitol [NG] as control) for 24 or 72 h. *C*: Schema of MGO and AGE metabolism. MGO as by-product from glucose metabolism can bind to proteins, lipids, and DNA, forming AGEs. GLO1 detoxifies MGO by converting it to D-lactate. *D*: Dot plot of the percent apoptotic cells in *db*/+ BMPCs treated with MGO, AGEs, or HG for 24 or 72 h (n = 5 per group). *E*: Representative scatter plots showing the distribution of Annexin-V^+/PI^- cells in *db*/+ BMPCs. *F*: Network formation quantification in *db*/+ BMPCs treated with MGO,

overexpress GLO1 in *db/db* BMPCs. Western blot analysis revealed significantly enhanced IRE1α protein expression and IRE1α phosphorylation (Fig. 5*A*), but *Ire1* mRNA expression levels in *db/db* BMPCs showed no change compared with Ad-GFP–infected control (Fig. 5*B*). A decrease in transcriptional activity of IRE1α after Ad-GLO1 infection was also observed, as measured by luciferase promotor reporter assay (Fig. 5*C*), indicating that augmentation of IRE1α protein and activation induced by GLO1 did not occur through transcriptional regulation but most likely by detoxifying MGO. Moreover, GLO1 protein in Ad-GLO1–infected *db/db* BMPCs was not affected by si-IRE1α transfection (Fig. 5*E*). Improved network formation driven by Ad-GLO1 infection displayed a moderate decrease by IRE1α siRNA (Fig. 5*F* and *G*). The overexpression of GLO1 and knockdown of IRE1α were confirmed by Western blot (Fig. 5*D*). Furthermore, using the same protocol as used for mouse BMPCs, we cultured human PCs from peripheral mononuclear cells in healthy individuals and patients with type 2 diabetes. PCs from lean healthy subjects expressed high levels of IRE1α as well as GLO1, whereas subjects with type 2 diabetes possessed low levels of both IRE1α and GLO1 in BMPCs (Fig. 5*H*). These data suggest that high GLO1 protein expression is associated with high IRE1α protein expression and that the levels of GLO1 dictate the expression of IRE1α.

BMPC Therapy With GLO1 Overexpression Accelerates Diabetic Wound Closure and Augments Wound Angiogenesis

We have established that healthy BMPCs can efficiently heal diabetic wounds, but diabetic BMPCs cannot achieve efficacy equal to that of their healthy counterparts because diabetic BMPCs are functionally impaired (31). We therefore examined whether genetically engineered diabetic BMPCs with enhanced GLO1 expression have better efficacy. First, our results indicate that diabetic mice receiving *db/db* BMPC therapy had significantly delayed wound closure compared with those receiving *db/+* BMPC therapy (Fig. 6*A* and *B*). Remarkably, GLO1 overexpression in *db/db* BMPCs showed accelerated wound closure compared with the diabetic control cell therapy, starting from day 4. On day 16 after surgery, the wounds receiving *db/db* BMPCs with GLO1 overexpression were clinically healed as evidenced by a slightly keratinized epithelial layer, but the wounds receiving control *db/db* BMPCs still exhibited an open wound area (Fig. 6*B*). We also examined the capillary density on the wound edge during wound healing. On day 6, when robust angiogenesis occurred, the wounds and adjacent skin were immunohistochemically stained with CD31. The numbers of capillary-like structures (stained brown) were much higher in wounds receiving *db/db* BMPCs with GLO1 overexpression than those receiving control *db/db* BMPCs (Fig. 6*C*), suggesting a robust angiogenic response induced by *db/db* BMPCs with GLO1 overexpression. Together, these data suggest that enhancing GLO1 expression in diabetic BMPCs improves their efficacy in treating diabetic wounds.

Augmentation of Tissue GLO1 Expression Improves Diabetic Wound Healing

To evaluate whether augmenting tissue GLO1 expression achieves equal or even better outcomes in diabetic wounds, we adopted two approaches to elevate tissue GLO1 levels during wound healing. First, immediately after wounding, Ad-GLO1 was injected into the wound edge to upregulate GLO1 expression, using Ad-GFP as a control (one application, 10^8 pfu/wound). In wounds receiving Ad-GLO1, we observed a dramatically improved closure rate compared with wounds receiving Ad-GFP (Fig. 7*A* and *C*). CD31 immunohistochemistry of day 6 wounds indicated improved capillary formation (Fig. 7*B*). The protein expression of GLO1 was measured on day 16 wound samples to ensure that tissue GLO1 remained high through observation (Fig. 7*D*). Second, we treated diabetic wounds with a small-molecule coformulation of 5 μmol/L tRES and 5 μmol/L HESP to induce GLO1 expression every other day (32). Western blot analysis confirmed increased levels of GLO1 protein expression in wound tissue (Fig. 7*H*). Diabetic wounds with tRES-HESP treatment showed significantly faster closure (Fig. 7*E* and *G*) with concomitantly more capillary formation than wounds treated with vehicle control (Fig. 7*F*). An increase in transcriptional activity of GLO1 after tRES-HESP treatment to *db/db* BMPCs was observed by luciferase promotor reporter assay (Fig. 7*I*). These experiments reveal that direct overexpression of tissue GLO1 effectively accelerates wound closure and restores angiogenesis in diabetic animals.

GLO1 Improves Wound Healing in Endothelial-Specific IRE1α Knockout Mice

Our in vitro experiments suggested that IRE1α$^{-/-}$ BMPCs exhibited significantly impaired function, which was reversed by GLO1 gene transfer. Furthermore, to test whether GLO1 can improve wound healing in IRE1α^{ECKO} mice, Ad-GLO1 was applied to the wound bed immediately after wounding. Our results showed that there was a delay in wound closure in IRE1α^{ECKO} mice compared with IRE1α$^{flox/flox}$ mice starting from day 6 (Fig. 8*A* and *B*). Meanwhile, capillary formation in IRE1α^{ECKO} wounds was aberrant relative to wounds in IRE1α$^{flox/flox}$ mice (Fig. 8*C*), suggesting the essentiality of IRE1α in angiogenesis.

AGEs, or HG for 24 or 72 h (n = 4 per group). *G*: Dot plot of migration assay of *db/+* BMPCs treated with MGO, AGEs, or HG for 24 or 72 h (n = 5 per group). *H*: Representative images of tube network formed by *db/+* BMPCs treated with MGO, AGEs, or HG for 24 or 72 h. Scale bar = 1,000 μm. *I*: Representative images of migration assay of *db/+* BMPCs treated with MGO, AGEs, or HG for 24 or 72 h. Scale bar = 200 μm. *$P < 0.05$ vs. controls; **$P < 0.01$ vs. controls.

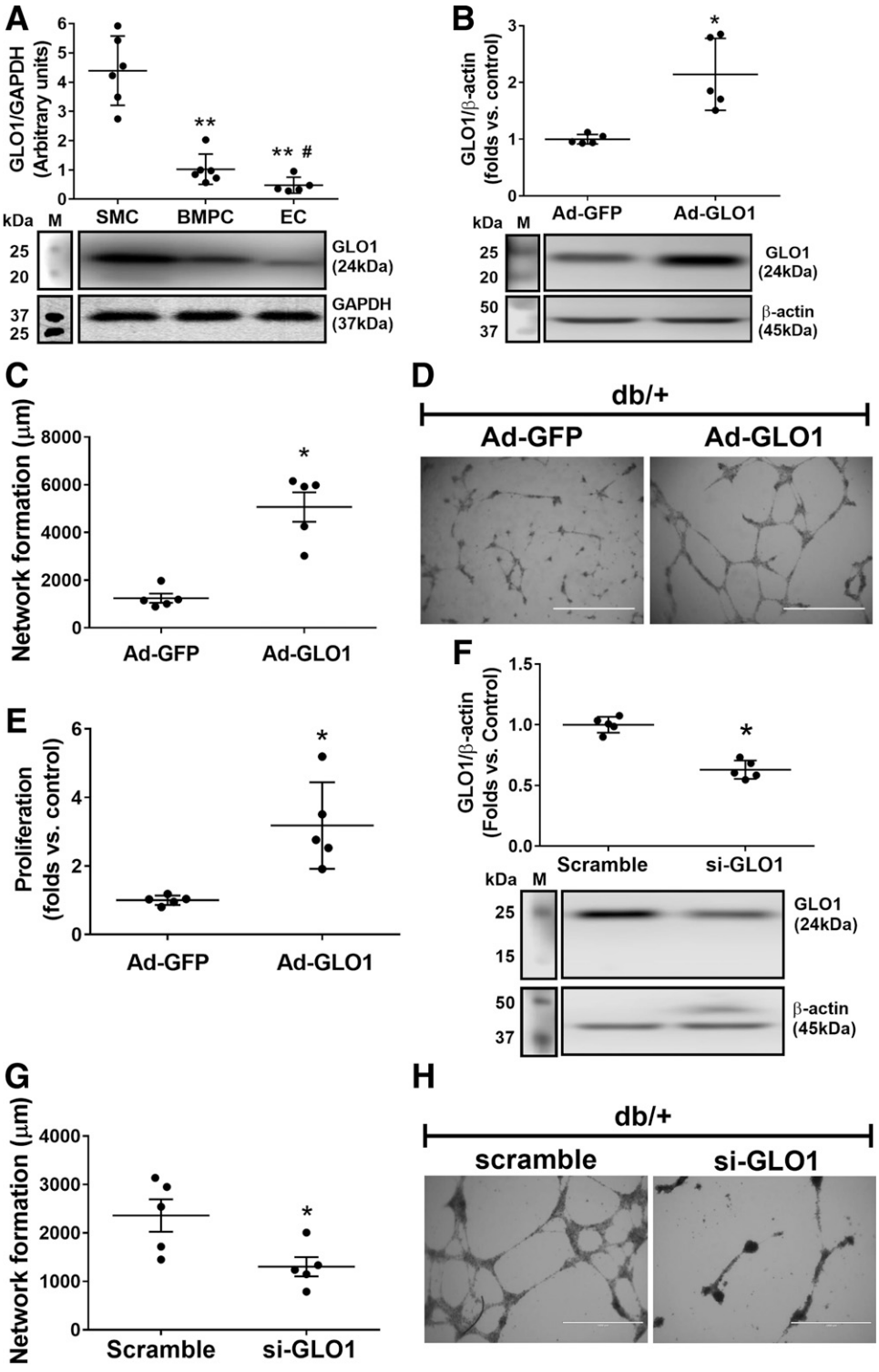

Figure 2—Augmentation of GLO1 improved BMPC function, whereas GLO1 deficiency caused BMPC dysfunction. *A*: GLO1 expression levels in SMCs, BMPCs, and endothelial cells (ECs) ($n = 5$ per group). $^{**}P < 0.01$ vs. SMC; $\#P < 0.05$ vs. BMPC. *B*: Western blot analysis of GLO1 protein in *db*/+ BMPCs infected with Ad-GLO1, using Ad-GFP as control ($n = 5$ per group). $^{*}P < 0.05$ vs. *db*/+ plus Ad-GFP. *C*: Dot plot of network formation quantification of *db*/+ BMPCs infected with Ad-GLO1 or Ad-GFP ($n = 5$ per group). $^{*}P < 0.05$ vs. *db*/+ plus Ad-GFP. *D*: Representative images of network formation in *db*/+ BMPCs infected with Ad-GLO1 or Ad-GFP ($n = 5$ per group). Scale bar = 1,000 μm. *E*: Proliferation of *db*/+ BMPCs infected with Ad-GLO1 or Ad-GFP ($n = 5$ per group). $^{*}P < 0.05$ vs. *db*/+ plus Ad-GFP. *F*: Western blot analysis of GLO1 expression level in *db*/+ BMPC transfected with si-GLO1 or scramble oligo ($n = 5$ per group). $^{*}P < 0.05$ vs. *db*/+ plus scramble. *G*: Network formation in *db*/+ BMPC transfected with si-GLO1 or scramble oligo ($n = 5$ per group). $^{*}P < 0.05$ vs. *db*/+ plus scramble. *H*: Representative images of *db*/+ BMPC transfected with si-GLO1 or scramble oligo. Scale bar = 1,000 μm. M, protein marker.

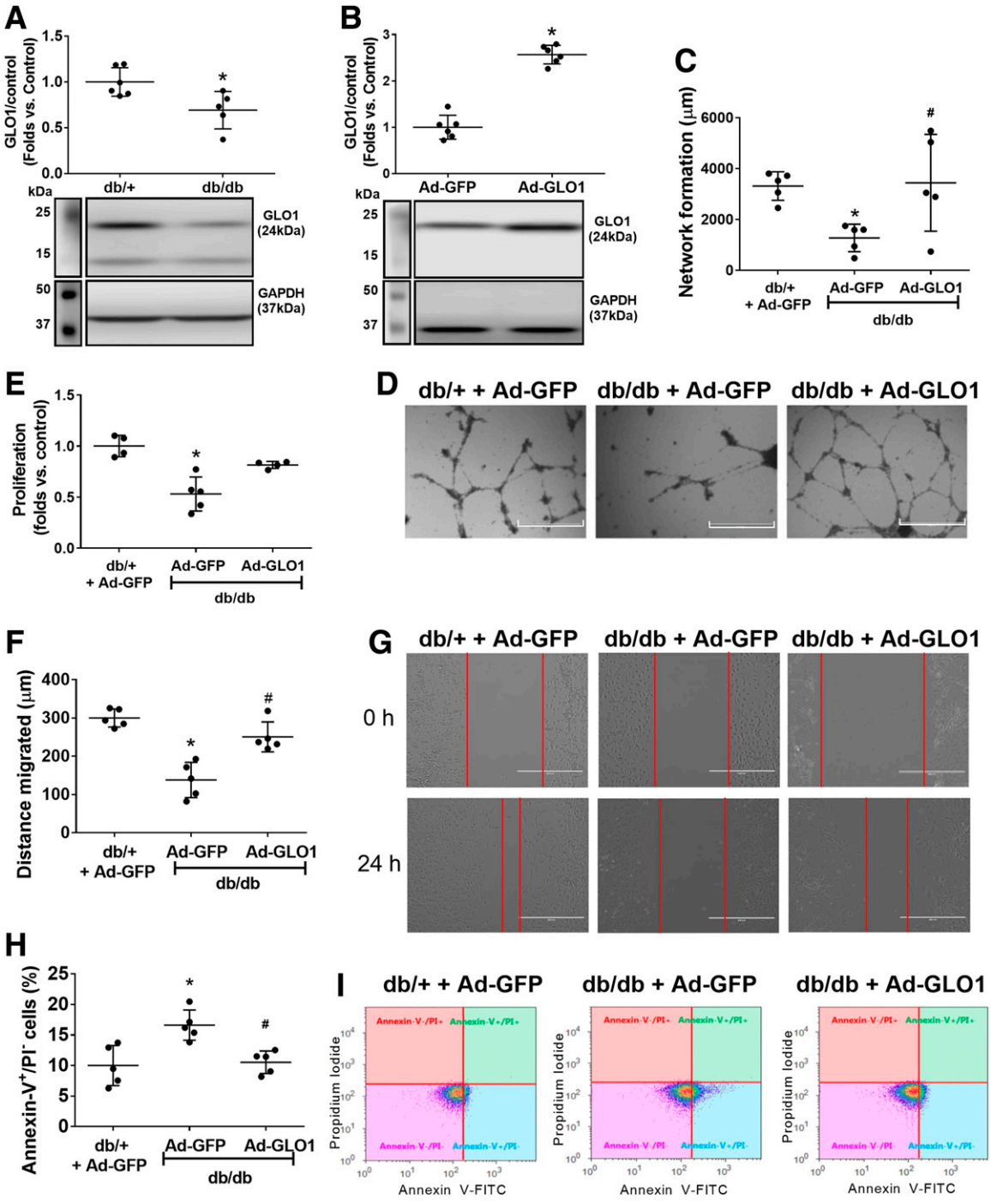

Figure 3—GLO1 overexpression rescued diabetes-induced BMPC dysfunction. *A*: Western blot analysis showing deficient expression levels of GLO1 in diabetic BMPCs compared with healthy controls ($n = 5$ per group). *$P < 0.01$ vs. *db*/+. *B*: Western blot analysis of GLO1 protein level in *db*/*db* BMPCs infected with Ad-GLO1, using *db*/*db* BMPC-infected Ad-GFP as diabetic control ($n = 5$ per group). *$P < 0.05$ vs. *db*/*db* plus Ad-GFP. *C*: Dot plot of network formation quantification of *db*/*db* BMPCs infected with Ad-GLO1 or Ad-GFP or *db*/+ BMPCs infected with Ad-GFP ($n = 5$ per group). *$P < 0.05$ vs. *db*/+ plus Ad-GFP; #$P < 0.05$ vs. db/db plus Ad-GFP. *D*: Representative images of network formation. Scale bar = 1,000 μm. *E*: Dot plot of proliferation assay of *db*/*db* BMPCs infected with Ad-GLO1 or Ad-GFP or *db*/+ BMPCs infected with Ad-GFP ($n = 5$ per group). *$P < 0.05$ vs. *db*/+ plus Ad-GFP. *F*: Dot plot of migration assay of *db*/*db* BMPCs infected with Ad-GLO1 or Ad-GFP or *db*/+ BMPCs infected with Ad-GFP ($n = 5$ per group). *$P < 0.05$ vs. *db*/+ plus Ad-GFP; #$P < 0.05$ vs. *db*/*db* plus Ad-GFP. *G*: Representative images of migration. Scale bar = 1,000 μm. *H*: Dot plot of the percent apoptotic cells in *db*/*db* BMPCs infected with Ad-GLO1 or Ad-GFP or *db*/+ BMPCs infected with Ad-GFP ($n = 5$ per group). *$P < 0.05$ vs. *db*/+ plus Ad-GFP; #$P < 0.05$ vs. *db*/*db* plus Ad-GFP. *I*: Representative scatter plots showing the distribution of Annexin-V^+/PI^- cells.

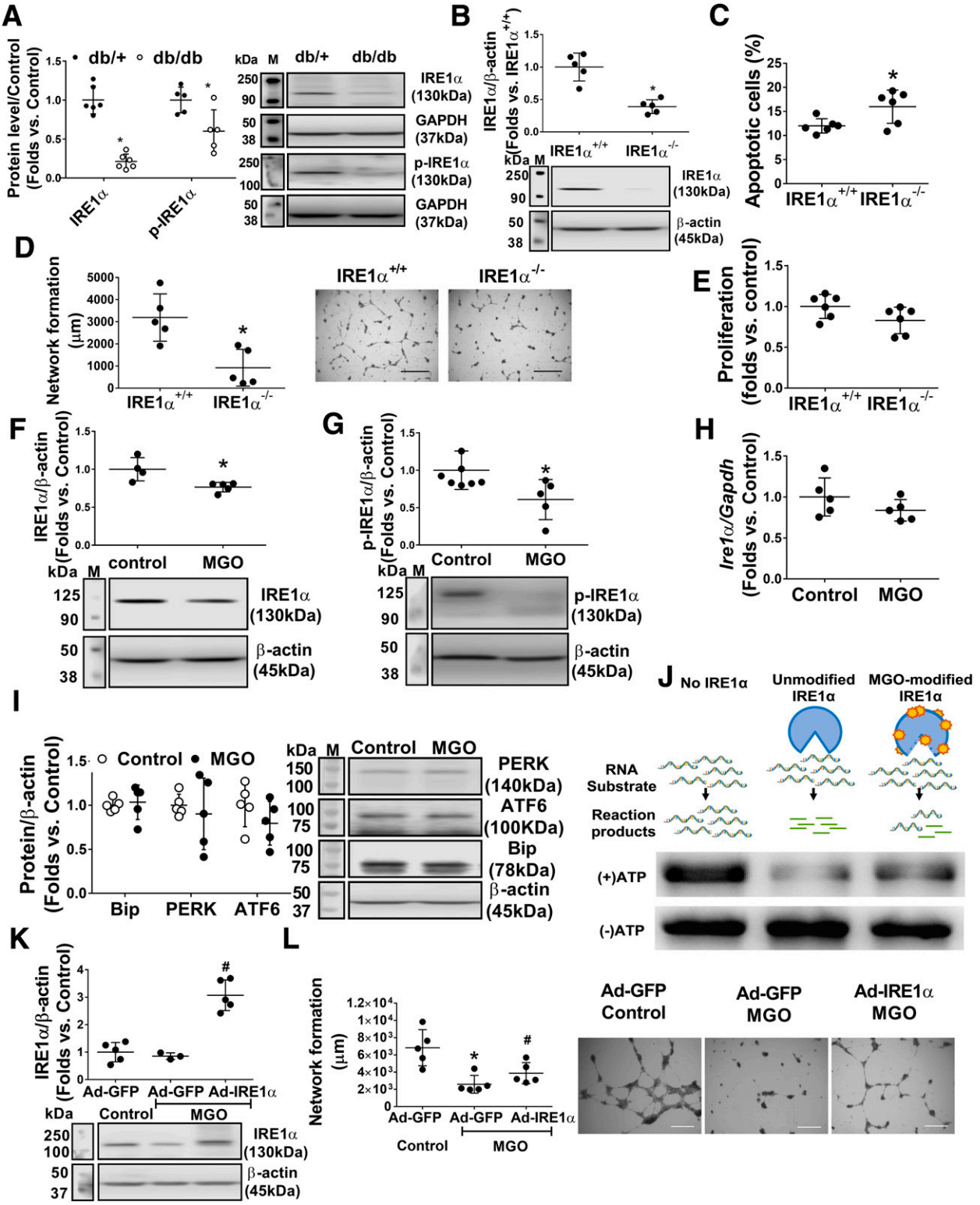

Figure 4— IRE1α deficiency contributes to BMPC dysfunction, and MGO suppresses IRE1α expression at the protein level. Overexpression of IRE1α rescues BMPC dysfunction after MGO exposure. *A*: Western blot analysis of expression levels of IRE1α and the phosphorylated form of IRE1α (p-IRE1α) in *db/db* and *db/+* BMPCs. Representative protein bands are shown ($n = 5$ per group). *$P < 0.05$ vs. *db/+*. *B*: Western blot analysis of IRE1α level in IRE1α$^{+/+}$ BMPCs infected with Ad-Cre (IRE1α$^{-/-}$) or Ad-GFP (IRE1α$^{+/+}$) ($n = 5$ per group). *$P < 0.05$ vs. IRE1α$^{+/+}$. *C*: Apoptosis of IRE1A$^{-/-}$ or IRE1α$^{+/+}$ BMPCs was evaluated by caspase 3/7 assay ($n = 5$ per group). *$P < 0.05$ vs. IRE1α$^{+/+}$. *D*: Network formation quantification of IRE1α$^{-/-}$ or IRE1α$^{+/+}$ BMPCs ($n = 5$ per group). *$P < 0.05$ vs. IRE1α$^{+/+}$. Representative pictures are shown. Scale bar = 1,000 μm. *E*: Proliferation of IRE1α$^{-/-}$ or IRE1α$^{+/+}$ BMPCs ($n = 5$ per group). *F*: Western blot analysis of IRE1α in *db/+* BMPCs exposed to 10 μmol/L MGO for 24 h ($n = 5$ per group). *$P < 0.05$ vs. control. *G*: Western blot analysis of p-IRE1 in *db/+* BMPCs exposed to 10 μmol/L MGO for 24 h ($n = 5$ per group). *$P < 0.05$ vs. control. *H*: Levels of *Ire1* mRNA in *db/+* BMPCs exposed to MGO ($n = 5$ per group). *I*: Western blot

Importantly, both wound healing and wound angiogenesis were significantly improved by GLO1 overexpression. Thus, GLO1 might sustain tissue repair through multiple pathways in addition to promoting IRE1α.

DISCUSSION

In this study, we showed that micromolar levels of MGO induce severe BMPC dysfunction. In contrast, only modest BMPC dysfunction is observed after prolonged exposure to high glucose or AGEs. We previously identified IRE1α as an important protein in BMPC-mediated angiogenesis (4), but the mechanistic basis of its functional impairment in diabetes remains largely unknown. MGO inhibited IRE1α function by directly binding to IRE1α protein, resulting in compromised RNase activity. GLO1 expression was decreased in diabetic BMPCs compared with that in normal BMPCs. Overexpression of GLO1 rescued BMPC functionality through the scavenging of MGO, with concomitant augmentation of IRE1α protein expression and activation. In an in vivo diabetic wound model, we observed a significantly improved efficacy of diabetic cell therapies with GLO1 overexpression or tissue GLO1 augmented by Ad-GLO1 gene transfer or with the small-molecule formulation of GLO1 inducers tRES and HESP. Overall, these observations suggest that by scavenging MGO, GLO1 can improve BMPC function in diabetes, facilitate angiogenesis, and rescue the compromised efficacy of diabetic cell therapies in wound healing. We have also identified IRE1α as one of the susceptible intracellular proteins modified by MGO (Fig. 8*D*).

Glycation stress is an important component of metabolic disorders. However, the role of reactive dicarbonyl intermediates such as MGO in tissue damage tends to be underappreciated primarily because most published studies use concentrations of MGO that far exceed estimated upper limits of plasma MGO levels in patients with diabetes (34,35). We suspect that serum in in vitro cell culture media serves as a sink to trap MGO, thereby significantly limiting the unbound MGO interactions with the cells. Using a transient serum-deprived cell culture protocol, we acquired evidence that MGO at micromolar concentrations caused immediate damage to BMPC function (Fig. 1), whereas high glucose or AGEs failed to induce similar damage. The data suggest that free reactive dicarbonyl species (RDS) are much more detrimental to BMPC function than hyperglycemia per se or AGEs, raising the question of whether monitoring glucose is sufficient to predict diabetes-related complications or comorbidity in the clinic. Glycated hemoglobin (HbA_{1c}) is one of the most studied glycated plasma proteins and is widely used to monitor glycemic control in the clinic (36). HbA_{1c} reflects average glucose levels during the preceding 12 weeks but does not provide direct information about unbound RDS accumulation. Recently, a retrospective report showed no association between baseline HbA_{1c} or change in HbA_{1c} and wound healing time in patients with diabetic foot ulcers (37). In this regard, detection of unbound RDS might serve as a better prognostic marker for tissue damage in patients with diabetes. Future studies are needed to explore the association between unbound RDS and tissue damage together with the development of an appropriate methodology to assess unbound RDS in tissue or body fluid.

Conformational changes induced by MGO modification can either damage or activate protein function or confer resistance to proteolysis (38,39). We found that MGO at micromolar levels directly inhibited IRE1α function (Fig. 4*F*, *G*, and *J*) but not two other ER stress sensors, PERK and ATF6 (Fig. 4*I*), or other functional proteins, such as endothelial nitric oxide synthase and VE growth factors (data not shown). This raises the possibility that IRE1α is a relatively vulnerable target of MGO modification. MGO binds to the arginine, lysine, and cysteine residues in proteins (6). The reaction of MGO with arginine and lysine produces stable products, whereas the reaction with cysteine produces reversible adducts. Human IRE1α protein consists of 977 amino acids, including 46 arginines, 56 lysines, and 15 cysteines (UniProt Knowledge Base O75460). There are several amino acid residues on IRE1α that are particularly important to the autophosphorylation (activation) and endoribonuclease activity of IRE1α. Many of these regions contain either arginine or lysine that can be modified by MGO (Supplementary Table 1). It would be interesting to identify the high-affinity sites of MGO adduction in IRE1α. The elevation of MGO or the dysfunctional ER stress response might in turn exacerbate hyperglycemia because the detrimental effects of excessive MGO or ER stress in pancreatic β-cells have been recognized in separate studies (11,22,23). Findings of the current study serve as a link between dicarbonyl stress and disruption of ER homeostasis and will provide a base

analysis of protein levels of PERK, ATF6, and Bip in *db*/+ BMPCs exposed to MGO ($n = 5$ per group). *J*: Agarose electrophoresis of IRE1α-mediated RNA cleavage assay of native and MGO-modified IRE1α. One microgram of in vitro–transcribed RNA (pre-miR-466:pre-miR-200 = 1:1) was used as RNA substrate of IRE1α. The cleavage reaction without ATP initiation was used as loading control. Left lane: RNA substrate without IRE1α incubation. Middle lane: spliced RNA substrate after native IRE1α incubation. Right lane: RNA substrate incubated with MGO-modified IRE1α. *K*: Western blot analysis of IRE1α protein expression in *db*/*db* BMPCs infected with Ad-IRE1α or Ad-GFP after exposure of 10 μmol/L MGO for 24 h (using H_2O as control) ($n = 5$ per group). #$P < 0.05$ vs. *db*/*db* plus Ad-IRE1α plus MGO. *L*: Network formation quantification of *db*/*db* BMPCs infected with Ad-IRE1α or Ad-GFP after MGO exposure ($n = 5$ per group). *$P < 0.05$ vs. *db*/*db* plus Ad-GFP plus control; #$P < 0.05$ vs. *db*/*db* plus Ad-GFP plus MGO. Representative images of tube network are shown. M, protein marker. Scale bar = 1,000 μm.

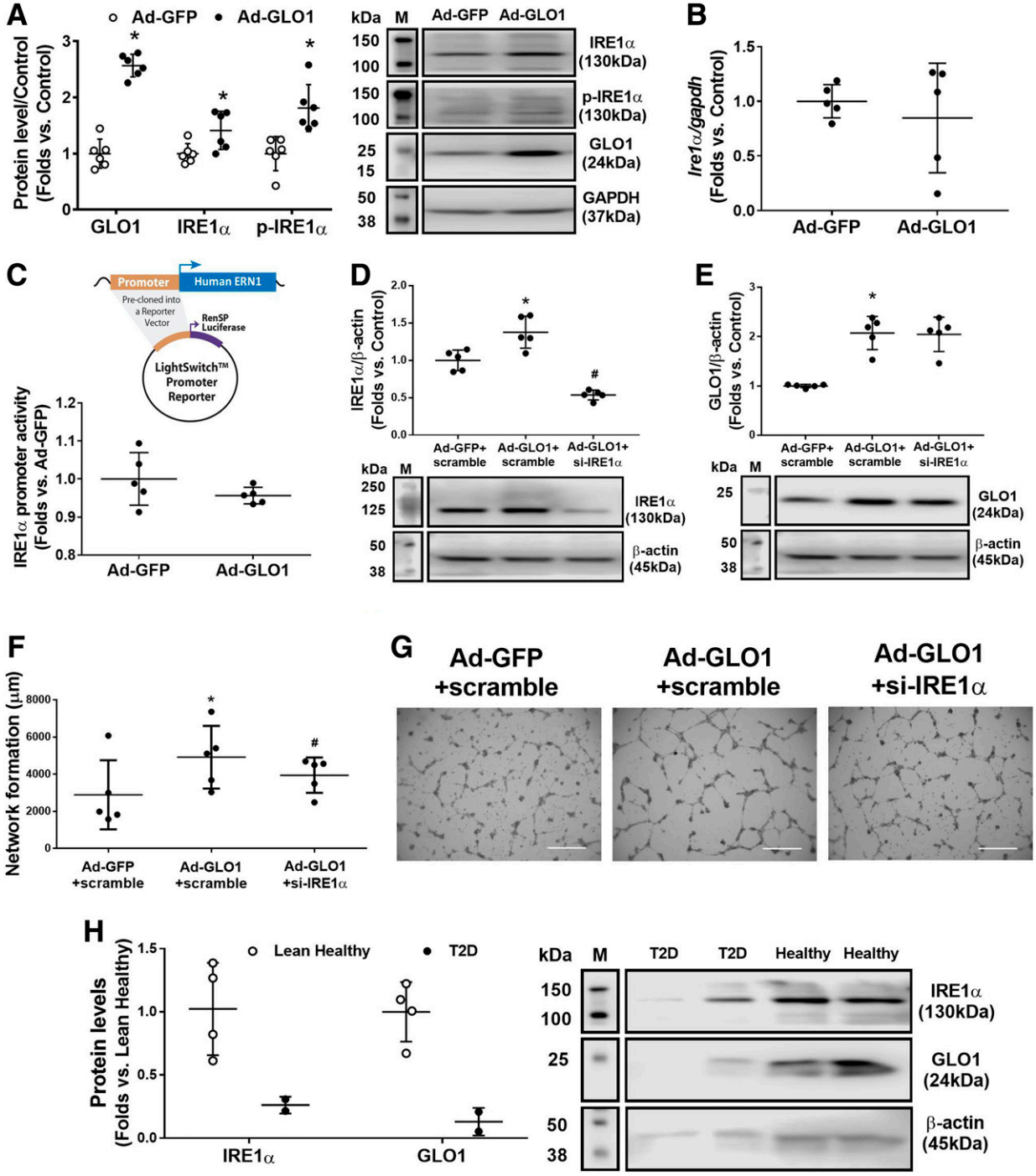

Figure 5—Overexpression of GLO1 augments IRE1α expression at the protein level. *A*: Western blot analysis of IRE1α and the phosphorylated form of IRE1α (p-IRE1α) protein levels after infection with Ad-GLO1 in *db/db* BMPCs, using *db/db* BMPCs infected with Ad-GFP as control ($n = 5$ per group). *$P < 0.05$ vs. *db/db* plus Ad-GFP. Representative protein bands are shown. *B*: Quantitative RT-PCR analysis of *Ire1* mRNA level in *db/db* BMPCs infected with Ad-GLO1 or Ad-GFP using *gapdh* as internal control ($n = 5$ per group). *C*: Luciferase promoter reporter assay of transcriptional activity of IRE1α in *db/db* BMPCs infected with Ad-GLO1 or Ad-GFP ($n = 5$ per group). Shown above the dot plot is the structure of LightSwitch Promoter Reporter with precloned oligonucleotides of human IRE1α promoter. *D*: Western blot analysis of IRE1α expression in GLO1-overexpressed *db/db* BMPCs transfected with si-IRE1α or scramble oligo, using Ad-GFP–infected and scramble oligo–transfected *db/db* BMPCs as control ($n = 5$ per group). *$P < 0.05$ vs. *db/db* plus Ad-GFP plus scramble; #$P < 0.05$ vs. *db/db* plus Ad-GLO1 plus scramble. *E*: Western blot analysis of GLO1 expression levels in *db/db* BMPCs with different gene manipulation ($n = 5$ per group). *$P < 0.05$ vs. *db/db* plus Ad-GFP plus scramble. *F*: Network formation quantification of GLO1-overexpressed *db/db* BMPCs transfected with si-IRE1α or scramble oligo, using Ad-GFP–infected and scramble oligo–transfected *db/db* BMPCs as control ($n = 5$ per group). *$P < 0.05$ vs. Ad-GFP plus scramble oligo; #$P < 0.05$ vs. Ad-GLO1 plus scramble oligo. *G*: Representative images of network formation. Scale bar = 1,000 μm. *H*: Western blot analysis of GLO1 and IRE1α protein expression in human PCs from peripheral mononuclear cells in healthy individuals ($n = 4$) and patients with type 2 diabetes (T2D) ($n = 2$). Representative bands are shown. M, protein marker.

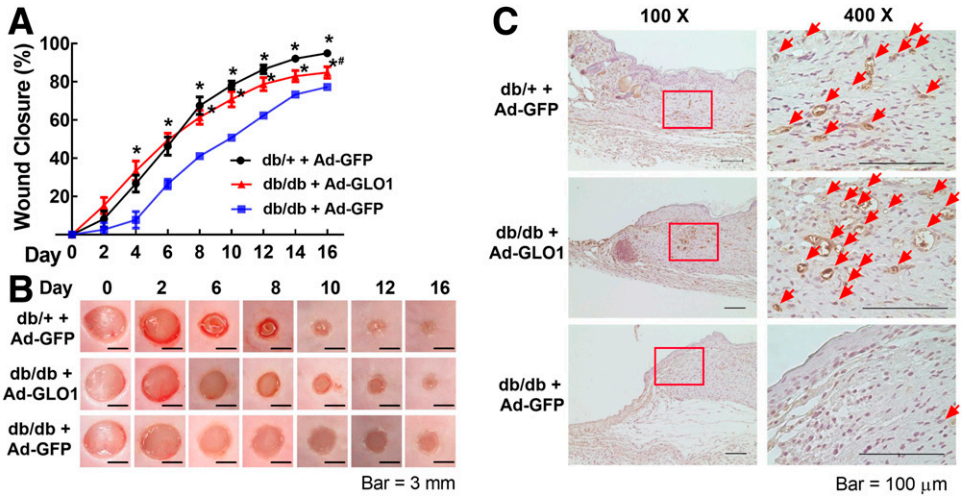

Figure 6—GLO1 improved diabetic BMPC therapy in wound healing in type 2 diabetic mice. For cell therapies, 1×10^6 *db/db* BMPCs infected with Ad-GLO1 or Ad-GFP were transplanted onto *db/db* wounds. *A*: Wound closure curves in *db/db* mice that received BMPC therapies ($n = 5$ per group). *B*: Representative images of cutaneous wounds taken on days 0, 6, 10, and 16 after wounding. *C*: Capillary formation as evaluated by CD31 staining (brown) in wounds that received cell therapies. Arrows indicate capillary-like structures at wound edge. Images on right are amplified from the region marked with a square on the left. *$P < 0.05$ vs. *db/db* plus Ad-GFP; #$P < 0.05$ vs. *db/+* plus GFP.

for better measurement of the in vivo exposure to reactive carbonyls.

GLO1 is the major enzyme that metabolizes MGO in mammalian cells (6). Energy-consuming cells, such as SMCs, use glucose to generate ATP, which inevitably generates RDS. Robust expression of GLO1 enables SMCs to remove MGO generated during glycolysis. However, endothelial cells and BMPCs are not equipped with such a strong glyoxalase defense system (Fig. 2*A*). Moreover, whereas healthy BMPCs are more capable of dealing with glycation stress than endothelial cells, diabetic PCs from animal and human subjects have lower GLO1 protein expressions (Figs. 4*A* and 5*H*). The imbalance between decreases in GLO1 expression and increases in MGO accumulation may play a critical role in BMPC dysfunction in a hyperglycemic environment. Indeed, impaired BMPC function was rescued by GLO1 overexpression (Fig. 3*C*–*I*). GLO1 overexpression significantly enhanced IRE1α expression and activation (phosphorylation) (Fig. 5*C*). However, the promoter activity of mRNA coding IRE1α and levels of mRNA transcripts of IRE1α remain unchanged (Fig. 5*B* and *D*), suggesting that GLO1 preserves IRE1α expression and activity at the posttranslational level by preventing adverse MGO-induced modifications. Conversely, IRE1α does not regulate GLO1 expression because GLO1 protein expression remains unchanged upon overexpression of IRE1α (Supplementary Fig. 2). The mechanism underlying reduced GLO1 protein expression in diabetic BMPCs is not clear. MGO exposure (at μmol/L levels) did not alter GLO1 protein expression (Supplementary Fig. 3). Aging contributes to GLO1 deficiency in wound healing (40), although no mechanism has been proposed. Interestingly, GLO1 siRNA led to significant inhibition of BMPC network formation under normal glucose conditions (Fig. 2*G*), suggesting the possibility that GLO1 modulates cellular activity independent of scavenging MGO. A previous report suggested that GLO1 suppresses tumor necrosis factor–induced transcriptional activity of nuclear factor-κB and expression of inflammatory genes in human embryonic kidney 293 cells (41). This proposed pathway may be a plausible mechanism in endothelial cell lineage. Investigations on how GLO1 interacts with the nuclear factor-κB promoter region (directly or indirectly) are needed. Despite these questions, accumulating evidence has shown the protective roles of GLO1 for endothelial cell function in vitro (42,43) and for endothelial PC recruitment for diabetic tissues (44,45) in vivo. GLO1-based interventions, either combined with cell therapies or not, were reported in streptozotocin-induced diabetic animal models with ischemic limbs (44,46,47). All these findings support the potential therapeutic values of alleviating glycation and oxidative stress in diabetic tissues.

A recent clinical trial showed that a novel small-molecule formulation, tRES and HESP, screened through ~100 dietary bioactive compounds exhibited the ability to increase GLO1 expression by enhancing the transcriptional activity of the antioxidant response element in GLO1 and reducing MGO protein glycation in 29 obese subjects (32). Our data revealed that the formulation also shows remarkable improvement in wound healing. The first attempt to use this formulation for topical wound treatment may accelerate clinical translation. Our animal studies provide supportive evidence that preventing MGO-induced protein glycation by enhancing GLO1 activity is a plausible approach for diabetic wound treatment.

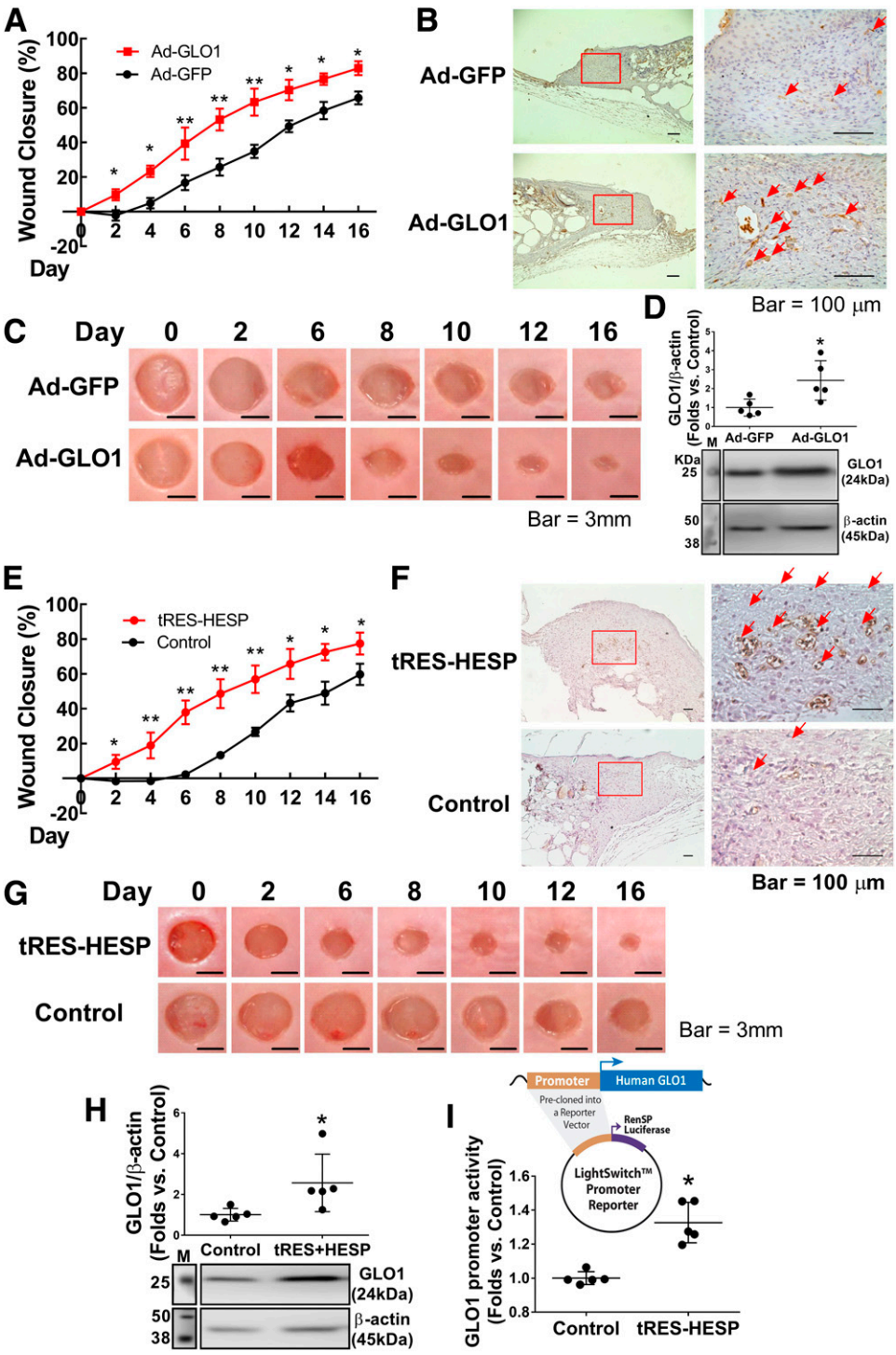

Figure 7— Local gene transfer of GLO1 or augmentation of GLO1 by coformulation of tRES- and HESP-improved diabetic wound healing. *A*: Wound closure curves in *db/db* mice that received local gene transfer ($n = 5$ per group). *$P < 0.05$, **$P < 0.01$ vs. *db/db* plus Ad-GFP. *B*: Capillary formation as evaluated by CD31 staining (brown) in wounds receiving gene transfer. The arrows indicate capillary-like structures at wound edge. Images on the right are amplified from the region marked with a square on the left. *C*: Representative images of cutaneous wounds. *D*: GLO1 expression levels in tissue at the edge of wounds in *db/db* mice that received gene transfer ($n = 5$ per group). *$P < 0.05$ vs. *db/db* plus Ad-GFP. *E*: Wound closure curves in *db/db* mice that received tRES-HESP coformulation or vehicle control (0.002% DMSO). *$P <$ 0.05 vs. *db/db* plus control, **$P < 0.01$ vs. control. *F*: Capillary formation as evaluated by CD31 staining (brown) in wounds. The arrows indicate capillary-like structures at wound edge. Images on the right are amplified from the region marked with a box on the left. *G*: Representative images of cutaneous wounds. *H*: GLO1 expression level in tissue at the edge of wounds that received tRES-HESP therapy ($n = 5$ per group). *$P < 0.05$ vs. control. *I*: Luciferase promoter reporter assay of transcriptional activity of GLO1 in *db/db* BMPCs treated with tRES-HESP coformulation showed that tRES-HESP enhanced GLO1 promotor activity ($n = 5$ per group). *$P < 0.05$ vs. control. Shown above the dot plot is the structure of LightSwitch Promoter Reporter with precloned oligonucleotides of human GLO1 promoter. M, protein marker.

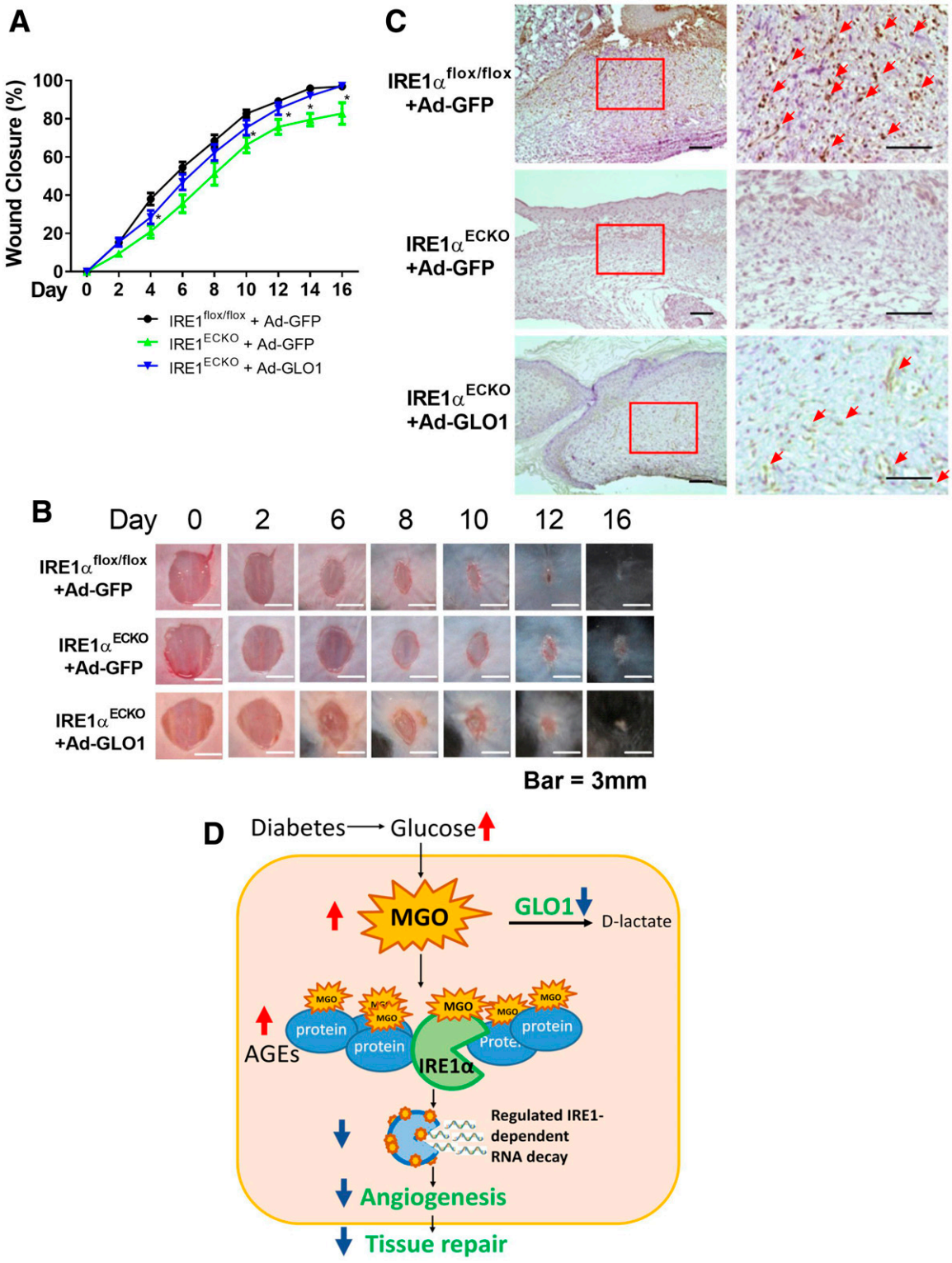

Figure 8— GLO1 gene transfer rescued impaired wound healing in IRE1α^{ECKO} mice compared with IRE1α$^{flox/flox}$ mice. For local gene transfer, 1×10^8 pfu Ad-GLO1 or Ad-GFP in 40 μL PBS were loaded onto the wounds. *A*: Wound closure curves in IRE1α^{ECKO} mice that received Ad-GLO1 ($n = 7$) or Ad-GFP ($n = 5$); IRE1α$^{flox/flox}$ mice that received Ad-GFP ($n = 8$) were set as controls. *$P < 0.05$ vs. IRE1α$^{flox/flox}$ plus Ad-GFP. *B*: Representative images of cutaneous wounds. *C*: Capillary formation as evaluated by CD31 staining (brown) in wounds that received gene transfer. The arrows indicate capillary-like structures at wound edge. Images on the right are amplified from the region marked with a square on the left. Scale bar = 100 μm. *D*: Proposed mechanism by which GLO1 improves compromised angiogenesis under diabetic conditions. Elevated blood glucose in patients with diabetes generates excessive MGO. By rapidly reacting with proteins, including IRE1α, MGO causes dysfunction of IRE1α RNase activity, leading to compromised angiogenesis and tissue repair. GLO1, as the main enzyme that metabolizes MGO, can decrease plasma concentrations of MGO, therefore facilitating angiogenesis by partly augmenting functional IRE1α protein levels.

There are several caveats to be considered regarding our findings. First, we identified IRE1α as one of the vulnerable protein targets of MGO. However, MGO targets almost any protein that has cysteine, arginine, and lysine residues. Extracellular matrix proteins are more susceptible to glycation or oxidation damage compared with circulating or intracellular proteins because they have relatively slow turnover rates (48). Proteomic analysis on MGO-modified intra/extracellular proteins will likely unveil more protein glycation hot spots in patients with diabetes. Second, MGO-induced BMPC dysfunction was investigated in this study, but MGO affects various cell types that participate in diabetic wound repair, including keratinocytes and fibroblasts (49,50). Although beyond the scope of the current study, it would be interesting to evaluate the impact of pathophysiological levels of MGO on these cell types. Finally, the pilot data using human blood samples did not permit a definitive conclusion on the relationship between GLO1 and IRE1α in peripheral vascular PCs. Efforts are ongoing to collect human specimens for further investigations. Nonetheless, our study highlights the underestimated role of highly reactive dicarbonyl intermediates in causing BMPC dysfunction, with IRE1α being a critical target. The data also reveal the detrimental effects of pathophysiologically relevant MGO exposure on cellular dysfunction and tissue damage in vitro and in vivo. Understanding the underappreciated role of RDS in diabetes and its subsequent detrimental impact on protein function may open a new paradigm for the investigation of mechanisms of wound pathogenesis and the development of therapeutic protocols.

Acknowledgments. The authors acknowledge the outstanding technical support for real-time PCR analyses provided by Dr. Fei Chen and technical assistance for BMPC isolation provided by Yihan Wang (both in the Department of Pharmaceutical Sciences at Wayne State University). The authors also thank the staff from the Department of Laboratory Animal Research at Wayne State University for providing excellent care for the animals.

Funding. This work was supported in part by National Institute of Diabetes and Digestive and Kidney Diseases grants R01-DK-090313 (to K.Z.); R01-DK-107666 and R01-DK-081750 (to Z.Y.); R01-DK-103185, R24-DK-110973, and R01-DK-113171 (to R.J.K.); and R01-DK-109036 (to J.-M.W.). This work also was supported by Wayne State University Undergraduate Research and Creative Projects (to M.O.) and Wayne State University Cardiovascular Research Institute Isis Award 2017 (to J.-M.W.). R.J.K. is a member of the University of California, San Diego, Diabetes Research Center (P30 DK063491) and adjunct professor in the Department of Pharmacology, University of California, San Diego.

Duality of Interest. No potential conflicts of interest relevant to this article were reported.

Author Contributions. H.L. conducted experiments, acquired data, analyzed data, and wrote the manuscript. M.O. conducted experiments, acquired data, and edited the manuscript. X.Z. assisted with editing the manuscript. K.Z. provided the key reagent, conceived the idea of IRE1α-mediated miR degradation, contributed to the discussion, and edited the manuscript. B.S. and Z.Y. provided clinical assistance for human sample collection, contributed to the discussion, and edited the manuscript. R.J.K. provided the key reagent and edited the manuscript. T.J.M. conceived the idea, contributed to the discussion, and edited the manuscript. J.-M.W. conceived the idea, designed the research studies, analyzed data, wrote the manuscript, and provided research funding. J.-M.W. is the guarantor of this work and, as such, had full access to all the data in the study and takes responsibility for the integrity of the data and the accuracy of the data analysis.

Data Availability. All data generated or analyzed during this study are included in the published manuscript (and Supplementary Data). The IRE1α floxed mice that support the findings of this study are available from R.J.K., but restrictions apply to the availability of these mice, which were used under license for the current study and therefore are not publicly available. IRE1α floxed mice may be available from the authors and/or R.J.K. upon reasonable request and with permission of R.J.K.

References

1. Centers for Disease Control and Prevention (CDC). Lower extremity disease among persons aged > or =40 years with and without diabetes–United States, 1999-2002. MMWR Morb Mortal Wkly Rep 2005;54:1158–1160

2. Asahara T, Murohara T, Sullivan A, et al. Isolation of putative progenitor endothelial cells for angiogenesis. Science 1997;275:964–967

3. Berezin AE. Endothelial progenitor cells dysfunction and impaired tissue reparation: the missed link in diabetes mellitus development. Diabetes Metab Syndr 2017;11:215–220

4. Wang JM, Qiu Y, Yang ZQ, Li L, Zhang K. Inositol-requiring enzyme 1 facilitates diabetic wound healing through modulating MicroRNAs. Diabetes 2017; 66:177–192

5. Desai K, Wu L. Methylglyoxal and advanced glycation endproducts: new therapeutic horizons? Recent Pat Cardiovasc Drug Discov 2007;2:89–99

6. Nigro C, Leone A, Raciti GA, et al. Methylglyoxal-glyoxalase 1 balance: the root of vascular damage. Int J Mol Sci 2017;18:188

7. McLellan AC, Thornalley PJ, Benn J, Sonksen PH. Glyoxalase system in clinical diabetes mellitus and correlation with diabetic complications. Clin Sci (Lond) 1994;87:21–29

8. Wang H, Meng QH, Gordon JR, Khandwala H, Wu L. Proinflammatory and proapoptotic effects of methylglyoxal on neutrophils from patients with type 2 diabetes mellitus. Clin Biochem 2007;40:1232–1239

9. Hanssen NMJ, Scheijen JLJM, Jorsal A, et al. Higher plasma methylglyoxal levels are associated with incident cardiovascular disease in individuals with type 1 diabetes: a 12-year follow-up study. Diabetes 2017;66:2278–2283

10. Hanssen NMJ, Westerink J, Scheijen JLJM, van der Graaf Y, Stehouwer CDA, Schalkwijk CG; SMART Study Group. Higher plasma methylglyoxal levels are associated with incident cardiovascular disease and mortality in individuals with type 2 diabetes. Diabetes Care 2018;41:1689–1695

11. Fiory F, Lombardi A, Miele C, Giudicelli J, Beguinot F, Van Obberghen E. Methylglyoxal impairs insulin signalling and insulin action on glucose-induced insulin secretion in the pancreatic beta cell line INS-1E. Diabetologia 2011;54: 2941–2952

12. Mukohda M, Okada M, Hara Y, Yamawaki H. Exploring mechanisms of diabetes-related macrovascular complications: role of methylglyoxal, a metabolite of glucose on regulation of vascular contractility. J Pharmacol Sci 2012;118:303–310

13. Rabbani N, Thornalley PJ. Glyoxalase in diabetes, obesity and related disorders. Semin Cell Dev Biol 2011;22:309–317

14. Genuth S, Sun W, Cleary P, et al.; DCCT Skin Collagen Ancillary Study Group. Glycation and carboxymethyllysine levels in skin collagen predict the risk of future 10-year progression of diabetic retinopathy and nephropathy in the diabetes control and complications trial and epidemiology of diabetes interventions and complications participants with type 1 diabetes. Diabetes 2005;54:3103–3111

15. Brouwers O, Niessen PM, Haenen G, et al. Hyperglycaemia-induced impairment of endothelium-dependent vasorelaxation in rat mesenteric arteries is mediated by intracellular methylglyoxal levels in a pathway dependent on oxidative stress. Diabetologia 2010;53:989–1000

16. Dhar A, Dhar I, Desai KM, Wu L. Methylglyoxal scavengers attenuate endothelial dysfunction induced by methylglyoxal and high concentrations of glucose. Br J Pharmacol 2010;161:1843–1856

17. Sousa Silva M, Gomes RA, Ferreira AE, Ponces Freire A, Cordeiro C. The glyoxalase pathway: the first hundred years... and beyond. Biochem J 2013;453:1–15
18. Rabbani N, Thornalley PJ. Dicarbonyl proteome and genome damage in metabolic and vascular disease. Biochem Soc Trans 2014;42:425–432
19. Skapare E, Konrade I, Liepinsh E, et al. Association of reduced glyoxalase 1 activity and painful peripheral diabetic neuropathy in type 1 and 2 diabetes mellitus patients. J Diabetes Complications 2013;27:262–267
20. Peng Z, Yang X, Qin J, et al. Glyoxalase-1 overexpression reverses defective proangiogenic function of diabetic adipose-derived stem cells in streptozotocin-induced diabetic mice model of critical limb ischemia. Stem Cells Transl Med 2017;6:261–271
21. Eizirik DL, Cardozo AK, Cnop M. The role for endoplasmic reticulum stress in diabetes mellitus. Endocr Rev 2008;29:42–61
22. Back SH, Kaufman RJ. Endoplasmic reticulum stress and type 2 diabetes. Annu Rev Biochem 2012;81:767–793
23. Lombardi A, Tomer Y. Interferon alpha impairs insulin production in human beta cells via endoplasmic reticulum stress. J Autoimmun 2017;80:48–55
24. Zhang K, Kaufman RJ. The unfolded protein response: a stress signaling pathway critical for health and disease. Neurology 2006;66(Suppl. 1):S102–S109
25. Hetz C, Martinon F, Rodriguez D, Glimcher LH. The unfolded protein response: integrating stress signals through the stress sensor IRE1α. Physiol Rev 2011;91:1219–1243
26. Upton JP, Wang L, Han D, et al. IRE1α cleaves select microRNAs during ER stress to derepress translation of proapoptotic caspase-2. Science 2012;338:818–822
27. Zhang K, Wang S, Malhotra J, et al. The unfolded protein response transducer IRE1α prevents ER stress-induced hepatic steatosis. EMBO J 2011;30:1357–1375
28. Li H, Liu J, Wang Y, et al. MiR-27b augments bone marrow progenitor cell survival via suppressing the mitochondrial apoptotic pathway in Type 2 diabetes. Am J Physiol Endocrinol Metab 2017;313:E391–E401
29. Chen J, Song M, Yu S, et al. Advanced glycation endproducts alter functions and promote apoptosis in endothelial progenitor cells through receptor for advanced glycation endproducts mediate overpression of cell oxidant stress. Mol Cell Biochem 2010;335:137–146
30. Kinsky OR, Hargraves TL, Anumol T, et al. Metformin scavenges methylglyoxal to form a novel imidazolinone metabolite in humans. Chem Res Toxicol 2016;29:227–234
31. Wang JM, Tao J, Chen DD, et al. MicroRNA miR-27b rescues bone marrow-derived angiogenic cell function and accelerates wound healing in type 2 diabetes mellitus. Arterioscler Thromb Vasc Biol 2014;34:99–109
32. Xue M, Weickert MO, Qureshi S, et al. Improved glycemic control and vascular function in overweight and obese subjects by glyoxalase 1 inducer formulation. Diabetes 2016;65:2282–2294
33. Wang JM, Chen AF, Zhang K. Isolation and primary culture of mouse aortic endothelial cells. J Vis Exp 2016;(118):e52965
34. Jan CR, Chen CH, Wang SC, Kuo SY. Effect of methylglyoxal on intracellular calcium levels and viability in renal tubular cells. Cell Signal 2005;17:847–855
35. Figarola JL, Singhal J, Rahbar S, Awasthi S, Singhal SS. LR-90 prevents methylglyoxal-induced oxidative stress and apoptosis in human endothelial cells. Apoptosis 2014;19:776–788
36. Koenig RJ, Peterson CM, Jones RL, Saudek C, Lehrman M, Cerami A. Correlation of glucose regulation and hemoglobin Alc in diabetes mellitus. N Engl J Med 1976;295:417–420
37. Fesseha BK, Abularrage CJ, Hines KF, et al. Association of hemoglobin A_{1c} and wound healing in diabetic foot ulcers. Diabetes Care 2018;41:1478–1485
38. Du J, Cai S, Suzuki H, et al. Involvement of MEKK1/ERK/P21Waf1/Cip1 signal transduction pathway in inhibition of IGF-I-mediated cell growth response by methylglyoxal. J Cell Biochem 2003;88:1235–1246
39. Nigro C, Raciti GA, Leone A, et al. Methylglyoxal impairs endothelial insulin sensitivity both in vitro and in vivo. Diabetologia 2014;57:1485–1494
40. Fleming TH, Theilen TM, Masania J, et al. Aging-dependent reduction in glyoxalase 1 delays wound healing. Gerontology 2013;59:427–437
41. de Hemptinne V, Rondas D, Toepoel M, Vancompernolle K. Phosphorylation on Thr-106 and NO-modification of glyoxalase I suppress the TNF-induced transcriptional activity of NF-kappaB. Mol Cell Biochem 2009;325:169–178
42. Rabbani N, Thornalley PJ. Glyoxalase 1 modulation in obesity and diabetes. Antioxid Redox Signal. 2 January 2018 [Epub ahead of print]. DOI: 10.1089/ars.2017.7424
43. Ahmed U, Dobler D, Larkin SJ, Rabbani N, Thornalley PJ. Reversal of hyperglycemia-induced angiogenesis deficit of human endothelial cells by over-expression of glyoxalase 1 in vitro. Ann N Y Acad Sci 2008;1126:262–264
44. Ceradini DJ, Yao D, Grogan RH, et al. Decreasing intracellular superoxide corrects defective ischemia-induced new vessel formation in diabetic mice. J Biol Chem 2008;283:10930–10938
45. Thangarajah H, Yao D, Chang EI, et al. The molecular basis for impaired hypoxia-induced VEGF expression in diabetic tissues. Proc Natl Acad Sci U S A 2009;106:13505–13510
46. Vulesevic B, McNeill B, Geoffrion M, et al. Glyoxalase-1 overexpression in bone marrow cells reverses defective neovascularization in STZ-induced diabetic mice. Cardiovasc Res 2014;101:306–316
47. Brouwers O, Yu L, Niessen P, et al. Glyoxalase-1 overexpression partially prevents diabetes-induced impaired arteriogenesis in a rat hindlimb ligation model. Glycoconj J 2016;33:627–630
48. Verzijl N, DeGroot J, Thorpe SR, et al. Effect of collagen turnover on the accumulation of advanced glycation end products. J Biol Chem 2000;275:39027–39031
49. Reichert O, Fleming T, Neufang G, et al. Impaired glyoxalase activity is associated with reduced expression of neurotrophic factors and pro-inflammatory processes in diabetic skin cells. Exp Dermatol 2017;26:44–50
50. Nowotny K, Castro JP, Hugo M, et al. Oxidants produced by methylglyoxal-modified collagen trigger ER stress and apoptosis in skin fibroblasts. Free Radic Biol Med 2018;120:102–113